# Fast Analysis of Nontree-Clock Network Considering Environmental Uncertainty by Parameterized and Incremental Macromodeling *

Hai Wang †, Hao Yu ‡, Sheldon X.-D. Tan †
†Department of Electrical Engineering, University of California, Riverside, CA 92521
‡Berkeley Design Automation, Santa Clara, CA 95054

## ABSTRACT

It is challenging to verify clock-skew for large-scale nontree clock network with environmental uncertainties such as supply voltage fluctuation and thermal temperature gradient. This paper presents a fast clock-skew analysis via parameterized incremental truncated-balanced-realization, called $piTBR$ method. Environmental uncertainties are parametrically and structurally added into the state equation of clock network. A compact macromodel is obtained by the subspace projection constructed from the singular value decomposition (SVD) of circuit output waveforms. To reduce the computational cost, we propose an incremental SVD method that only needs to partially update the projection matrix by analyzing the perturbed output waveform owning to environmental uncertainties. Experiments on a number of clock networks show that compared with the macromodeling by the fast TBR method, our method reduces the computational cost in the order of 100× with a similar accuracy. In addition, compared with the macromodeling by the Krylov-subspace-based method, our method reduces the waveform error by 2× with a similar runtime.

## 1. INTRODUCTION

Verifying clock skew, thus timing, under non-ideal environmental conditions is critical to design a robust high performance VLSI circuits [1, 2, 3, 4, 5, 6, 7]. As shown in [2] interconnect perturbations in clock trees can cause as much as 25% variation in clock skew. As the advance of VLSI technology has resulted in high-current density and power dissipation, it in turn leads to a high temperature-gradient within a chip. Because clock is globally routed over the chip, the temperature variation can bring significant skew variations [8, 5, 9, 6] as interconnect resistance is linearly perturbed with the temperature gradient. Moreover, the high-current in power delivery results in nonnegotiable IR drop and $L\frac{dI}{dt}$ noise. As a result, the fluctuation in supply voltage can also lead to perturbations to the clock-skew through clock drivers.

To counter the skew variation from environmental uncertainties, the perturbation-based deferred-merge-embedding (DME) method in [5, 6] modifies merging points for the tree-structure to minimize the skew variation. Compared with the clock-tree structure, the non-tree structure is found more robust under skew variations. The reason is that additional paths are provided for the signal to reach the clock sink nodes such that the variations can be compensated. The hybrid-network in [3] applied a top (root) level mesh to drive multiple clock trees in the lower (leaf) level. Recently, [4] added cross-links to convert a clock tree to a non-tree. Unlike the tree-structured network, there could be more than one clock-driver at inputs for a non-tree-structured network. More importantly, the efficient iterative algorithm for tree-structures can not be applied for the non-tree clock-network such as clock-meshes. The calculation of clock skew is expensive for non-tree clock-network during the sign-off stage.

Generally, the difficulties of clock-skew verification lie in twofold. Firstly, the post-layout physical model, contains of huge amount of extracted parasitic, would significantly increase the complexity of the model. Secondly, the environmental uncertainties from supply voltage and temperature, which form different timing corners or statical timing distributions, would perturb the clock-network and further complicate the verification of clock-skew. It is thus imperative to find a fast analysis for the non-tree clock-network considering environmental uncertainties.

In [3], a hierarchical macromodeling by the Krylov-subspace-based model-order-reduction (MOR) is applied to find the compact representation for parasitic. [7] improves the macromodeling by taking account of the input clock waveform information via a weighted reduction based on input harmonics. However, the Krylov-subspace-based macromodeling only has a localized accuracy yet a multi-point expansion will lead to more computing cost and larger sized models. An accurate macromodeling to calculate clock-skew hence needs a better control of the global error.

As an alternative macromodeling, the fast truncated-balanced-realization method, PMTBR, [10, 11] finds the dominant state by applying a singular-value-decomposition (SVD) to globally sampled waveforms under impulse inputs (called Grammian). It has a better global error-control than Krylov-subspace-based approaches. Recently, the fast TBR method, called $ETBR$, was proposed to reduce power grid networks with many ports by performing the reduction on both system matrices and input signals [12]. ETBR was shown to be more accurate and flexible than the Krylov based reduction-simulation methods [13, 14]. Nevertheless, the cost of SVD in EBR is high as it requires a full decomposition whenever the network changes or the input changes.

In this paper, we propose a fast clock-skew analysis via a parameterized incremental truncated-balanced-realization (piTBR) method. It improves the PMTBR and ETBR method [10, 11, 12] by an incremental SVD analysis that partially update the macromodel using those incremental changes at outputs, i.e., sensitivities.

The flow of piTBR is briefly reviewed as follows. We formulate a structured state-matrix to parametrically add the environmental uncertainties into the nominal state-matrix. Then, we apply a spectrum representation of input signals by fast Fourier transformation (FFT), and directly sample the nominal response and their sensitivities at outputs in frequency domain. With the structured output waveforms, we perform the TBR reduction with use of an incremental singular-value-decomposition (iSVD), which only analyzes the updated sensitivities every time when there exists environmental fluctuations. This can dramatically reduces the cost of SVD during TBR and is the primary contribution of our paper. Moreover, we apply a structured reduction to calculate both of the nominal response (skew) and its sensitivity (skew variation). As such, it would guide designers how to reduce the skew variation. In addition, our approach can consider the variation and its spatial correlation from both of the network and

*The work of Hai Wang and Sheldon X.-D. Tan is funded in part by NSF CAREER Award No. CCF-0448534, in part by NSF grant under No. OISE-0623038 and in part by National Natural Science Foundation of China (NSFC) grant under No. 60828008.

978-1-4244-2749-9/09/$25.00 ©2009 IEEE

the input. Therefore, our approach is more flexible to be applied in the verification of clock-skew under environmental uncertainties. Experiments show that compared to the macromodeling by the fast TBR method, our method reduces the computational cost in the order of 100X with a similar accuracy. Compared to the macromodeling by the Krylov-subspace-based method, our method reduces the waveform error by 2X with a similar runtime.

The rest of the paper is organized as follows. We first review the background of model order reduction by Krylov-subspace and truncated balanced realization in Section 2. We present a parameterized TBR method in Section 3 with a parameterization procedure for the environmental uncertainty, a frequency sampling of input spectrum and a structured TBR reduction. In Section 4, we introduce an incremental SVD method to speedup the parameterized TBR. We present the overall algorithm and the result in Section 6 and conclude the paper in Section 7.

# 2. BACKGROUND

## 2.1 State Matrix of Clock Network

The high-speed clock-network needs to be actually modeled by the distributed RLC model. The extracted RLC netlists can be described by a linear network in the modified nodal analysis (MNA) as

$$\mathcal{G}x(t) + \mathcal{C}\frac{dx(t)}{dt} = \mathcal{B}u(t), \tag{1}$$

or in frequency-domain (s) by

$$(\mathcal{G} + s\mathcal{C})x(s) = \mathcal{B}u(s), \tag{2}$$

where $\mathcal{G}$ and $\mathcal{C}$ ($\in \mathcal{N} \times \mathcal{N}$) are state-matrices for RLC elements, $x$ is the state-variable for nodal-voltage and Branch-current, and $\mathcal{B}$ ($\in \mathcal{N} \times p$) is the adjacent matrix describing the network connection with $p$ inputs sources $u$ ($\in p \times 1$).

## 2.2 Model Order Reduction by Truncation Balanced Realization

The post-layout extraction usually results in a RLC network with huge dimension. To find a compact model with dominant state-variables, model order reduction (MOR) is one solution. In general, MOR finds a small dimensioned matrix $Q$ ($\in \mathcal{N} \times K$) with $q < \mathcal{N}$, and applies a two-side projection to reduce the dimension of the original model from $\mathcal{N} \times \mathcal{N}$ to $q \times q$.

As shown in [15, 16], the dominant state variables are related to the block Krylov subspace, composed by the locally expanded moments. The limitations of this approach however, are two-fold. Firstly, its error can not be globally controlled as moments are obtained by expanding at one specified frequency $s_0$. Secondly, its effectiveness is limited as the order of matched moments is reversely dependent on the number of inputs.

Differently, the MOR by truncated-balanced realization (TBR) has a better global-error control by constructing the projection matrix from globally sampled waveforms. The fast TBR method [10, 11], called as PMTBR method, constructs the projection matrix by $n$-sampled waveforms at outputs in frequency-domain

$$Z = [z(s_1), z(s_2), ..., z(s_n)] \quad \in \mathcal{N} \times p \times n \tag{3}$$

where

$$z(s_i) = [\mathcal{G} + s_i\mathcal{C}]^{-1}\mathcal{B}. \tag{4}$$

The singular-value-decomposition (SVD) is then applied to $Z$ and its first-K SVD-vectors are $U \in \mathcal{N} \times K$, $S \in K \times K$ and $V \in K \times p \times n$ from

$$Z =^{svd} U \cdot S \cdot V. \tag{5}$$

By applying orthonormalization to $U$, a projection matrix $Q_S$ ($\in \mathcal{N} \times K$), called as system-projection, is constructed to reduce the original system by.

$$\hat{\mathcal{G}} = Q_S^T \mathcal{G} Q_S,\ \hat{\mathcal{C}} = Q_S^T \mathcal{C} U,\ \hat{\mathcal{B}} = Q_S^T \mathcal{B}. \tag{6}$$

However, similar as Krylov subspace methods, the fast TBR methods still have low efficiency issues for circuit with large numbers of ports. Since the dimension of sampled waveform $Z$ still depends on the number of ports $p$, its cost of SVD and the order of $K$ are large when the number of ports $p$ is large.

## 2.3 Extended Reduction Considering Inputs

The computational cost introduced by inputs can be reduced if we also project the input-port matrix $\mathcal{B}$ by a projection matrix $Q_I$ ($\in p \times K$)

$$B = \mathcal{B}Q_I \quad \in N \times K. \tag{7}$$

$Q_I$ is called as input-projection. It represents $K$ principal inputs that dominates the system response.

$Q_I$ can be extracted based on the input correlations. The works in [17, 18] find $Q_I$ from the SVD-vectors of the system transfer function $\mathcal{B}^T(\mathcal{G} + s\mathcal{C})^{-1}\mathcal{B}$. The works in [10] proposes to first extract the input correlation, and then find $Q_I$ from the SVD-vectors of the input correlation matrix directly.

To apply the input-projection once, the input correlation would necessary be stationary. Otherwise, the projection needs to be reconstructed all the time. As the patterns of input waveforms are usually known during sign-off for the clock or power-delivery network, the EKS/IEKS method [13, 14] uses the input current-vector [19]

$$\mathcal{J}(s) = \mathcal{B}u(s) = \begin{bmatrix} u_1 \\ u_2 \\ ... \\ u_p \\ ... \end{bmatrix} \quad \in \mathcal{N} \times 1 \tag{8}$$

instead of the input-port matrix $\mathcal{B}$ during the reduction. The port-dependence is disappeared as the dimension of $\mathcal{J}(s)$ is $\in \mathcal{N} \times 1$.

In the extended truncated balanced realization (ETBR) method [12], the input-current-vector-based reduction construct the projection matrix from the SVD of

$$X = [x(s_1), x(s_2), ..., x(s_n)] \quad \in \mathcal{N} \times n \tag{9}$$

where

$$x(s_i) = [\mathcal{G} + s_i\mathcal{C}]^{-1}\mathcal{J}(s_i). \tag{10}$$

As $X$ is $\in \mathcal{N} \times n$, its SVD cost can be much reduced. Moreover, the redundant input information such as the spatial correlation is still included in $\mathcal{J}$.

Different from the MOR to reduce the transfer function, the reduction with right-hand inputs needs to apply reduction every time when inputs or networks change. Note that our objective is to calculate the clock skew under incremental changes under environmental uncertainties. As such, both of the network and the input will change under the temperature and the supply fluctuation, respectively. Based on this observation, in this paper, we apply the ETBR reduction once to the nominal network $\mathcal{G}$ and $\mathcal{C}$ with the nominal input vector $\mathcal{J}$. Then, with a structured parameterization to stamp environmental uncertainties, we will develop an incremental SVD method that can update the reduction by only analyzing the changes in the outputs, i.e., the sensitivities.

# 3. PARAMETERIZED MACROMODEL OF CLOCK NETWORK

## 3.1 Parameterization with Environmental Uncertainty

Broadly speaking, the skew variation of the clock-network can be classified into the environment uncertainty and process uncertainty. This paper deals with the environmental uncertainty, which is the result of increased power dissipation and decreased voltage supply. There are two ways to treat the environmental uncertainty. One assumes that the fluctuation from the environment such as temperature can be still characterized as the worst-case corner [2, 4, 5, 9]. The other [6] applies a stochastic characterization of the environmental fluctuation. Our method supports both of above characterizations for the environmental uncertainty, and we assume the characterization of the environmental uncertainty is already provided for the following skew and skew variation analysis.

Moreover, note that the time-scale of thermal perturbation is in milli-second, quite different from the time-scale of supply voltage perturbation in nano-second. As such, the perturbed state vector $x_N$ by temperature is naturally not correlated to the perturbed state vector $x_I$ by supply voltage. Hence, we can separately apply the perturbation analysis as follows.

When a clock wire experiences a temperature gradient, the unit-length resistance $r_{unit}$ is [8]

$$r_{unit}(x, y, t) = \rho_0 \cdot [1 + \beta \cdot T(x, y, t)]. \quad (11)$$

where $\rho_0$ is the unit-length resistance at $0^oC$, and $\beta$ is the temperature coefficient of resistance $(1/^oC)$. Systematically, we denote the perturbation to the overall nominal state-matrix $\mathcal{G}$ is $\delta\mathcal{G}$ $(\in \mathcal{N} \times \mathcal{N})$.

The according perturbed MNA by temperature becomes

$$(\mathcal{G} + \delta\mathcal{G} + s\mathcal{C}) \cdot (x + \delta x_N) = \mathcal{J}. \quad (12)$$

By reorganizing the terms in both sides according to the perturbation order up to the first order, (12) leads to

$$\begin{aligned}(\mathcal{G} + s\mathcal{C}) \cdot x &= \mathcal{J} \\ (\mathcal{G} + s\mathcal{C}) \cdot \delta x_N + \delta\mathcal{G} \cdot x &= 0. \end{aligned} \quad (13)$$

The high-order perturbation terms can be included similarly as handling process variations in [20].

The fluctuation in supply voltage can lead to small perturbation to drivers, i.e., the input waveforms to the clock network. We denote the perturbation to the overall nominal input-vector $\mathcal{J}$ as $\delta\mathcal{J}$ $(\in \mathcal{N} \times 1)$.

The according perturbed MNA by input becomes

$$(\mathcal{G} + s\mathcal{C}) \cdot (x + \delta x_I) = \mathcal{J} + \delta\mathcal{J}. \quad (14)$$

Similarly, by reorganizing the terms in both sides according to the perturbation order up to the first order, (12) leads to

$$\begin{aligned}(\mathcal{G} + s\mathcal{C}) \cdot x &= \mathcal{J} \\ (\mathcal{G} + s\mathcal{C}) \cdot \delta x_I &= \delta\mathcal{J}. \end{aligned} \quad (15)$$

The high-order impact to $x$ from $\mathcal{J}$ can be added by the superposition.

As such, we can formulate a parameterized state-matrix

$$\left( \begin{bmatrix} \mathcal{G} & 0 & 0 \\ 0 & \mathcal{G} & 0 \\ \delta\mathcal{G} & 0 & \mathcal{G} \end{bmatrix} + s \begin{bmatrix} \mathcal{C} & 0 & 0 \\ 0 & \mathcal{C} & 0 \\ 0 & 0 & \mathcal{C} \end{bmatrix} \right) \begin{bmatrix} x \\ \delta x_I \\ \delta x_N \end{bmatrix} = \begin{bmatrix} \mathcal{J} \\ \delta\mathcal{J} \\ 0 \end{bmatrix} \quad (16)$$

using a new state variable composed by the nominal $x(s)$ and its sensitivity $\delta x_N(s)$ with respect to the network change and $\delta x_I(s)$ with respect to the input change.

Due to the block-triangular structure in the augmented state-matrices, the nominal state-variable

$$x = (\mathcal{G} + s\mathcal{C})^{-1} \cdot \mathcal{J} \quad (17)$$

and its sensitivities

$$\delta x_I = (\mathcal{G} + s\mathcal{C})^{-1} \cdot \delta\mathcal{J} \quad (18)$$

$$\delta x_N = -(\mathcal{G} + s\mathcal{C})^{-1} \cdot \delta\mathcal{G} \cdot x \quad (19)$$

can be solved efficiently by the block-backward substitution. as there is only one LU-factor of $\mathcal{G} + s\mathcal{C}$. The overall response is can be simply calculated by $x + \delta x_I + \delta x_N$. In addition, as shown later on, such a structured formulation to separate sensitivities from the nominal response leads to an efficient incremental SVD update.

## 3.2 Input Harmonic Sampling

As the measurement of the clock skew distribution is performed to the the steady-state response, the output waveform can be measured under inputs of different harmonics [7]. Therefore, instead of applying an error-prone polynomial or rational polynomial fitting of the time-domain waveform as in [14], the Fourier transformation can be applied by expanding the waveform with the fundamental harmonic as the clock frequency, i.e. $\omega_0 = 2\pi f_0$.

Assume the Fourier expansion of the input $\mathcal{J}(t)$ is

$$\mathcal{J}(t) = \sum_{k=0}^{N} \mathcal{J}(k\omega_0) e^{jk\omega_0 t}, j = \sqrt{-1}, k = 1, .., n \quad (20)$$

where $\omega_0$ is the fundamental clock frequency, and $\mathcal{J}(k\omega_0)$ is the weight of $k$th harmonic.

Define $s_k = j \cdot k \cdot \omega_0$, then the $n$-sampled frequency-domain waveforms are

$$\begin{bmatrix} x(s_1) & x(s_2) & \cdots & x(s_n) \\ \delta x_I(s_1) & \delta x_I(s_2) & \cdots & \delta x_I(s_n) \\ \delta x_N(s_1) & \delta x_N(s_2) & \cdots & \delta x_N(s_n) \end{bmatrix} \quad (21)$$

with

$$\begin{aligned} x(s_k) &= (\mathcal{G} + s_k\mathcal{C})^{-1} \cdot \mathcal{J}(s_k) \\ \delta x_I(s_k) &= (\mathcal{G} + s_k\mathcal{C})^{-1} \cdot \delta\mathcal{J}(s_k) \\ \delta x_N(s_k) &= -(\mathcal{G} + s_k\mathcal{C})^{-1} \cdot \delta\mathcal{G} \cdot x(s_k). \end{aligned} \quad (22)$$

Note that the PMTBR method [10] needs a selective sampling procedure with weights according to the input bandwidth. Our reduction together with the right-hand input vector, however, intrinsically contains the weighted input information. Here the order of sampling $n$ needs to ensure the perturbed $\delta\mathcal{J}$ is in the sampling bandwidth. Moreover, to accurately construct the projection from SVD of waveforms, more sampling data are preferred. This may cause memory storage problem for large-scale test cases. As such, a column-scaling is applied to scale each entry in one column by the maximum in the same column. Those small entries are then truncated if its relative magnitude is smaller than one user specified threshold.

## 3.3 Structured Projection

A flat projection matrix $Q$ $(\in 3\mathcal{N} \times K)$ can be constructed from the first-K SVD-vectors $\mathcal{U}$ by:

$$\begin{bmatrix} x(s_1) & x(s_2) & \cdots & x(s_n) \\ \delta x_I(s_1) & \delta x_I(s_2) & \cdots & \delta x_I(s_n) \\ \delta x_N(s_1) & \delta x_N(s_2) & \cdots & \delta x_N(s_n) \end{bmatrix} =^{SVD} \mathcal{U} \cdot \mathcal{S} \cdot \mathcal{V}, \quad (23)$$

where $\mathcal{U} \in 3\mathcal{N} \times K$, $S \in K \times K$ and $V \in K \times n$.

However, directly applying such a flat projection matrix as in [10, 11] to structured state-matrices in (16) would destroy the block-triangular structure. This would prevent us to apply the cost-efficient incremental SVD update discussed in Section 4. Similar as [9, 6], this paper applies a structured projection during TBR as follows.

Partition the flat projection matrix $Q$ into $Q_0$, $Q_I$ and $Q_N$

$$Q = \begin{bmatrix} Q_0 \\ Q_I \\ Q_N \end{bmatrix} \quad (24)$$

according to the row-size of $x$, $x_I$ and $x_N$, respectively.

Further orthonormalize $Q_0$, $Q_I$ and $Q_N$ with each other, and construct a structured projection matrix $\mathcal{Q}$ by

$$\mathcal{Q} = \begin{bmatrix} Q_0 & 0 & 0 \\ 0 & Q_I & 0 \\ 0 & 0 & Q_N \end{bmatrix}. \quad (25)$$

Such a structured matrix will preserve the block-triangular structure during the projection in (6). In addition, the sensitivities can be still employed for optimization procedure after the reduction.

# 4. SPEEDUP BY INCREMENTAL SVD

In this Section, we discuss two incremental SVD (iSVD) methods: the exact iSVD and the fast iSVD. The fast iSVD is an approximated SVD method. As shown by experiments, the fast iSVD is faster than the exact iSVD yet with a similar error.

## 4.1 Exact iSVD

Due to the structured formulation, the output waveforms can be denoted by

$$\begin{bmatrix} X \\ dX \end{bmatrix} = \begin{bmatrix} x(s_1) & x(s_2) & \cdots & x(s_n) \\ \delta x_I(s_1) & \delta x_I(s_2) & \cdots & \delta x_I(s_n) \\ \delta x_N(s_1) & \delta x_N(s_2) & \cdots & \delta x_N(s_n) \end{bmatrix}, \quad (26)$$

where $X$ $(\in \mathcal{N} \times n)$ is the nominal waveform and $dX$ $(\in \mathcal{N} \times n)$ is the perturbation by environmental fluctuations composed by

$dX_I$ and $dX_N$. Clearly, here only $dX$ changes with the environmental fluctuation, and $X$ is the constant after the first SVD. Therefore, fully decomposing $[X\ dX]^T$ by SVD every time would be expensive. An incremental SVD is needed to only perform the decomposition to the newly updated data $dX$.

Many fast SVD methods are developed in the literature [21, 22, 23]. They avoid the full decomposition of the entire matrix by estimating an appropriate low-rank approximation with the partial calculation of the data. However, none of them can be directly applied to our problem. In this paper, we introduce an incremental SVD method as follows.

Assume the SVD of $X$ is

$$X =^{svd} U \cdot S \cdot V \tag{27}$$

with $U \in \mathcal{N} \times K$, $S \in K \times K$ and $V \in K \times n$.

Define $L$ by projecting $dX$ ($\in 2\mathcal{N} \times n$) along the SVD-vector $V^T$ ($n \times K$)

$$L = dX \cdot V^T = \begin{bmatrix} dX_I \cdot V^T \\ dX_N \cdot V^T \end{bmatrix} \quad \in 2\mathcal{N} \times K \tag{28}$$

Its orthogonal component $H$ is

$$H = dX - L \cdot V = \begin{bmatrix} dX_I \cdot (I - V^T \cdot V) \\ dX_N \cdot (I - V^T \cdot V) \end{bmatrix} \quad \in 2\mathcal{N} \times n. \tag{29}$$

The QR decomposition of $H$ is

$$H =^{qr} Q \cdot R. \tag{30}$$

Because

$$dX = Q \cdot R + L \cdot V, \tag{31}$$

the following identity can be derived

$$\begin{bmatrix} U & 0 \\ 0 & I \end{bmatrix} \begin{bmatrix} S & 0 \\ L & Q \end{bmatrix} \begin{bmatrix} V \\ R \end{bmatrix} = \begin{bmatrix} U \cdot S \cdot V \\ L \cdot V + Q \cdot R \end{bmatrix} = \begin{bmatrix} X \\ dX \end{bmatrix} \tag{32}$$

where $I$ is the identity matrix.

Therefore, the incremental SVD can be performed only to the updated columns and rows in $dX$ as follows.

Apply SVD to the middle matrix by

$$\begin{bmatrix} S & 0 \\ L & Q \end{bmatrix} =^{svd} U' \cdot S' \cdot V'. \tag{33}$$

Then, since

$$U'' \cdot S'' \cdot V'' = \begin{bmatrix} X \\ dX \end{bmatrix}, \tag{34}$$

only following updates

$$U'' = \begin{bmatrix} U & 0 \\ 0 & I \end{bmatrix} U', \tag{35}$$

$$S'' = S', \tag{36}$$

and

$$V'' = V' \begin{bmatrix} V \\ R \end{bmatrix} \tag{37}$$

are needed, where $U''$ is employed as the projection matrix. We call this method as the *exact incremental SVD*.

## 4.2 Fast iSVD

The above exact iSVD can exactly produce

$$\begin{bmatrix} X \\ dX \end{bmatrix} = U'' \cdot S'' \cdot V''. \tag{38}$$

However, as usually only $U''$ is the part we are interested in for the projection, we further present a *fast iSVD* method to perform the partial analysis of $dX$ and then update $U$ only.

As shown by our experiments, given the updated $dX$ from environmental fluctuations, its projection along singular-vector $V^T$, i.e., $L$ ($\in 2\mathcal{N} \times K$) is found to be a good approximation as the update to $U$ ($\mathcal{N} \times K$)

$$U'' = \begin{bmatrix} U \\ L \end{bmatrix}. \tag{39}$$

The reason is that when the system is perturbed incrementally, it will not largely modify the direction of the dominant state-vector such as $V^T$. In other words, we can still approximately extract the contribution of $dX$ to $U$ by projecting $dX$ along $V^T$.

Though the new $U''$ is not orthonormalized from the above construction, it will be orthonormalized later on when constructing the structured projection. Compared to the exact iSVD, the fast iSVD avoids the additional cost of a SVD and QR decomposition, and only has a cost in the matrix multiplication when building $L$. This is inexpensive when waveforms are sparsely compressed.

# 5. ALGORITHM AND RESULTS

## 5.1 Overall piTBR Algorithm

PARAMETERIZED AND INCREMENTAL TRUNCATED BALANCED REALIZATION METHOD (PITBR)

**Inputs:** $\mathcal{G}$, $\mathcal{C}$, $\mathcal{J}(t)$, $n$ and $K$
1. Compute $\delta\mathcal{G}$ and $\delta\mathcal{J}$ according to temperature-gradient and power-supply fluctuation
2. Convert all input signals $\mathcal{J}(t)$ into $\mathcal{J}(s)$ using FFT with $n$ harmonics
3. Sample $n$ waveforms: $x(s_k)$ and its sensitivities: $\delta x_I(s_k)$, and $\delta x_N(s_k)$ by (22)
4. Form matrices $X = [x(s_1), \ldots, x(s_n)]$, $dX_I = [\delta x_I(s_1), \ldots, \delta x_I(s_n)]$, and $dX_N = [\delta x_N(s_1), \ldots, \delta x_N(s_n)]$ with a sparse compression
5. If first-time, perform full SVD $[X; dX_I; dX_N] = \mathcal{U} \cdot \mathcal{S} \cdot \mathcal{V}$; else perform iSVD update $[X; dX_I; dX_N] = U'' \cdot S'' \cdot V''$
6. Goto 1 whenever there is new environmental fluctuations
7. Partition and orthonormalize $U''$ into structured $\mathcal{Q}$
8. Project and reduce $\hat{\mathcal{G}} = \mathcal{Q}^T\mathcal{G}\mathcal{Q}$, $\hat{\mathcal{C}} = \mathcal{Q}^T\mathcal{C}\mathcal{Q}$, $\hat{\mathcal{J}} = \mathcal{Q}^T\mathcal{J}$
9. Calculate skew from $x$ and its sensitivities from $\delta x_I$ and $\delta x_N$
**Outputs:** Skew and skew variation

In this subsection, we summarize the flow of piTBR method in Algorithm 1. Given the nominal state matrices ($\mathcal{G}$ and $\mathcal{C}$) of the clock network, specified sampling number-n and SVD order-K, the algorithm first calculates the network perturbation $\delta\mathcal{G}$ and input perturbation $\delta\mathcal{J}$ from provided temperature-gradient and power-supply fluctuations. Then, it applies FFT ($O(nlogn)$) to input signals and calculate the weighted sampling at output waveforms and their sensitivities according to (eqn:sample). As the augmented state matrix is lower-block triangular, the cost primarily comes from the LU decomposition of nominal state matrices ($O(\mathcal{N}^{1.2})$). The waveforms and their sensitives are folded together after a spare compression. A full SVD with order-K ($O(\mathcal{N}nK^2)$) [22] is applied if it is the first time, and an incremental SVD (iSVD with $O(\mathcal{N}nK)$) [23] is applied afterwards. The procedure repeats when there exists successive updates of environmental fluctuations. After the reduction, the skew and its variation are calculated from the reduced macromodel.

## 5.2 Experimental Results

The proposed piTBR algorithm is implemented in Matlab. All experimental data is measured on an Intel duel-core 2.0GHZ PC with 2GB cache. The PMTBR based variational analysis with a single input vector is used for the comparison. The sparse SVD (SVDPACK) in Matlab is used to analyze the sparsely compressed waveform (by a threshold 1e-5). The Krylov-subspace-based EKS method in [14] is implemented to compare. A chip with size $5cm^2$ is divided into a uniform grid to place the clock network and sample its temperature variations. The temperature maps at nodes of the grid are obtained from a micro-architecture level thermal simulation. The unit resistance $r_0 = 0.03\Omega/mum$ and $\beta = 0.007$ are used to calculate the perturbed network change, where $\beta$ is the temperature coefficient of resistance. Moreover, a clock signal with 1V Vdd, 1ns period and 0.1ns falling/rising time is used. About up to 10%Vdd random voltage fluctuation is randomly added in each clock period of the clock input. It represents the power supply fluctuation. In addition, the macromodel is used to generate the transient voltage response and its sensitivities, and then to calculate the clock skew and skew variation. The waveforms are measured at 50% Vdd for the skew.

| 1 | 2 | 3 | 4 | 5 | 6 | 7 | 8 | 9 | 10 | 11 | 12 | 13 | 14 |
|---|---|---|---|---|---|---|---|---|---|---|---|---|---|
| Ckt | node | port | order | sample | solve | eks | | fast-isvd | | exact-isvd | | full-svd | |
| | | | | time(s) | time(s) | time(s) | error | time(s) | error | time(s) | error | time(s) | error |
| rlc-mesh1 | 105 | 5 | 10 | 0.07 | 0.04 | 0.05 | 0.84% | 0.01 | 0.65% | 0.02 | 0.60% | 0.06 | 0.61% |
| rlc-mesh2 | 369 | 21 | 40 | 0.10 | 0.41 | 0.61 | 1.35% | 0.04 | 0.84% | 0.46 | 0.81% | 0.73 | 0.82% |
| rlc-mesh3 | 1377 | 85 | 60 | 0.29 | 1.56 | 3.90 | 1.40% | 0.15 | 1.19% | 3.87 | 1.16% | 14.3 | 1.16% |
| rlc-mesh4 | 15939 | 341 | 100 | 1.95 | 7.49 | 28.4 | 5.32% | 1.15 | 2.75% | 7.29 | 2.04% | 921 | 2.02% |
| rlc-mesh5 | 20865 | 1365 | 100 | 32.4 | 31.7 | 142 | NA | 4.48 | NA | 73 | NA | NA | NA |

**Table 1: Scalability comparison of runtime and skew-error for piTBR using incremental SVDs (exact and fast), the TBR using full SVD and the Krylov-subspace-based EKS method.**

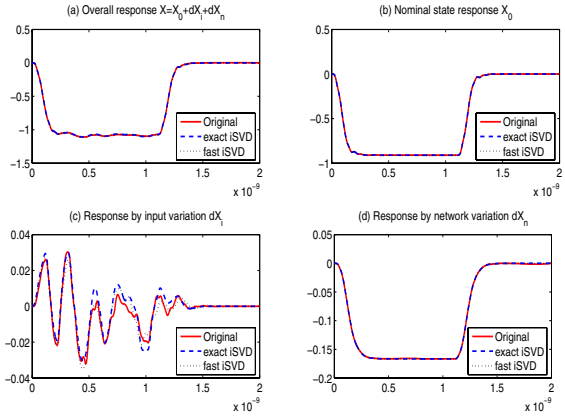


**Figure 1: Accuracy comparison by the original model and the macromodels by the exact iSVD and the fast iSVD. The waveforms are the overall response, nominal response, and first-order sensitivity. The first-order sensitivity $dX$ is in different magnitude-scale from the nominal value $X$.**

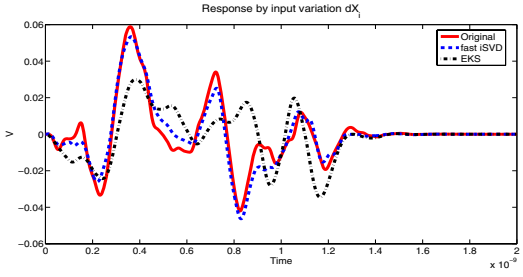


**Figure 2: Accuracy comparison by the original model and the macromodels by the Krylov-subspace-based EKS and the fast iSVD. The waveform is the first-order sensitivity due to the supply voltage perturbation.**

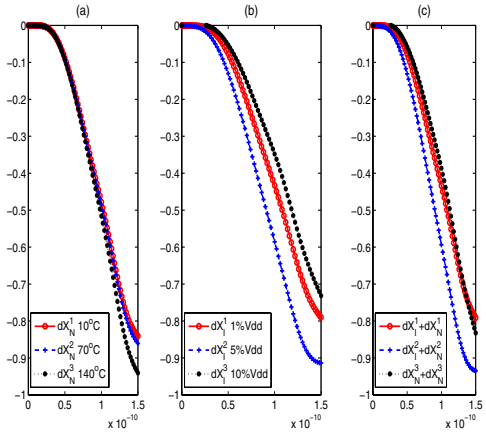


**Figure 3: Skew variation under temperature-caused network change $dX_N$ and supply-caused input change $dX_I$.**

### 5.2.1 *Accuracy of piTBR*

We first show the accuracy comparison of waveforms for the exact and the macromodels by piTBR using exact iSVD and fast iSVD in time-domains, respectively. A clock network with 1377 nodes and 85 ports is used with $70^oC$ temperature change, and 5%Vdd input perturbations. 100 sampling points are used to sample the waveform in frequency domain, and the SVD with order of 40 is applied to analyze the waveform.

Fig. 5.2 (a) compares the overall responses ($x_0 + dx_I + dx_N$), (b) compares the nominal responses ($x_0$), (c) compares the variations ($dx_I$) due to the input fluctuation by power-supply, and (d) compares the variations ($dx_N$) due to the network fluctuation by temperature-gradient. Clearly, compared to the exact model without using macromodel, both of macromodels by the exact iSVD and the fast iSVD can accurately catch the delay/skew (50%Vdd) yet about 61X (1.16s vs. 61.23s) times faster. Moreover, with the provided nominal response $x_0$ and its sensitivities i.e., the variations $dx_I$ and $dx_N$, the designers can easily modify their designs iteratively to reduce the skew variations.

For the same example above, Fig. 5.2 further compares the time-domain waveform $dX_I$s due to the input variation for the exact, the macromodels by the fast iSVD and the Krylov-subspace-based EKS method with the same model order at a different port. Clearly, as the macromodel by TBR method is constructed by globally sampling the waveform, it has a better accuracy than the Krylov-subspace-based method.

### 5.2.2 *Clock Skew Variation*

We then study the skew variation under different types of perturbations: purely by the temperature-gradient fluctuation; purely by the power-supply fluctuation; and by the combination of temperature and supply. For the same circuit above, we generate the various time-domain waveforms using macromodels by piTBR with order of 40.

Fig. 3 (a) shows the skew variation under the temperature

gradient with the following changes: $10^oC$, $70^oC$ and $140^oC$. It shows about 6% skew variation under the $140^oC$ temperature change. Moreover, Fig. 3 (b) shows the skew variation under the supply fluctuation with the following changes: 1%Vdd, 5% Vdd and 10% Vdd. It shows about 11% skew changes under the 5% Vdd perturbation. In addition, as shown by Fig. 3 (c) the combined environmental fluctuations the clock skew can have up to 14% variations under both temperature and supply fluctuations for the combined fluctuation 2.

### 5.2.3 Runtime Scalability

We further study the scalability of runtime and skew-error comparison among the piTBR with incremental SVD (exact iSVD and fast iSVD), the PMTBR with the single input vector, and the Krylov-subspace-based EKS method. A few of RLC meshes for clock network with increased size and port-number are used. The skew-error here is defined as the relative difference between the skew by the exact and the one by the macromodel. The runtime here includes the time of waveform sampling (Column 5), the time of solving reduced macromodel (Column 6), and the time of constructing the macromodel. Specifically, Column 7-8 show the time of Krylov-subspace-based iteration to construct macromodel, and the skew-error of EKS method. Column 7-8 show the SVD-time to construct macromodels and the skew-error of piTBR with the fast iSVD, column 9-10 show the same of piTBR with the exact iSVD, Column 11-12 show the same of PMTBR with full-SVD.

As shown by the table, the larger the size of waveform, the larger the cost to reapply the full SVD under environmental fluctuations. As iSVD only analyzes the incrementally added rows, it has a better scalability for large sized circuits than the full SVD. For a RLC circuit with 15939 nodes and 341 ports, iSVD shows up to 103X (2.83s vs 291s) runtime reduction in SVD with the similar waveform error (less than 1.5%).

Moreover, compared to the EKS method, the TBR methods show better accuracy of skew-error due to the global waveform sampling. For the same RLC mesh above, the TBR method reduces the skew-error by 2X. In addition, the computational cost of TBR is dramatically reduced by the incremental SVD. The exact iSVD has a similar cost as EKS method and the fast iSVD is even faster than the Krylov-subspace-based method.

## 6. CONCLUSIONS

The environmental uncertainties can introduce clock-skew variations. This paper presents a fast skew analysis for nontree clock network to consider uncertainties from the temperature-gradient and the power-supply fluctuations. It calculates the clock-skew based on a parameterized and incremental truncated-balanced realization method, called as piTBR. Compared to the existing macromodeling, our method is more flexible to be embedded within the skew-verification for large-scale clock networks. It introduces a structured state matrix to parametrically describe the network change by temperature and the input change by supply, simultaneously. This formulation has two advantages. Firstly, it facilitates an incremental SVD algorithm to reduce the computational cost in TBR methods. Secondly, it leads to a macromodel with both nominal value of skew and its sensitivity with respect to environmental changes. They can be utilized in optimization of the clock network. In addition, as the project matrix in TBR method is obtained by globally sampling the waveform, it leads to a more accurate macromodel than the one by the Krylov-subspace-based method. Our piTBR method reduces the runtime by 100X with a similar error compared to the full SVD based TBR method, and reduces the waveform error by 2X with a similar runtime compared to the Krylov-subspace-based method.

## 7. REFERENCES


[1] J. Cong, A. B. Kahng, C.-K. Koh, and C.-W. A. Tsao, "Bounded-skew clock and Steiner routing," *ACM TODAES*, 1997.

[2] Y. Liu, S. Nassif, L. Pileggi, and A. Strojwas, "Impact of interconnect variations on the clock skew of a gigahertz microprocessor," in *ACM/IEEE DAC*, 2000.

[3] H. Su and S. Sapatnekar, "Hybrid structured clock network construction," in *IEEE/ACM ICCAD*, 2001.

[4] A. Rajaram, J. Hu, and R. Mahapatra, "Reducing clock skew variability via cross links," in *ACM/IEEE DAC*, 2004.

[5] M. Cho, S. Ahmed, and D. Z. Pan, "TACO: Temperature aware clock-tree optimization," in *IEEE/ACM ICCAD*, 2005.

[6] H. Yu, Y. Hu, C. Liu, and L. He, "Minimal skew clock embedding considering time variant temperature variation," in *ACM ISPD*, 2007.

[7] X.Ye, P. Li, M.Zhao, R.Panda, and J.Hu, "Analysis of large clock meshes via harmonic-weighted model order reduction and port sliding," in *IEEE/ACM ICCAD*, 2007.

[8] A. H. Ajami, K. Banerjee, and M. Pedram, "Modeling and analysis of nonuniform substrate temperature effects on global ULSI interconnects," *IEEE TCAD*, pp. 849–861, 2005.

[9] H. Yu, J. Ho, and L. He, "Simultaneous power and thermal integrity driven via stapling in 3D ICs," in *IEEE/ACM ICCAD*, 2006.

[10] J. Phillips and L. Silveira, "Poor Man's TBR: A simple model reduction scheme," *IEEE TCAD*, pp. 43–55, 2005.

[11] J. Phillips, "Variational interconnect analysis via PMTBR," in *IEEE/ACM ICCAD*, 2004.

[12] D. Li, S. X.-D. Tan, and B. McGaughy, "ETBR: Extended truncated balanced realization method for on-chip power grid network analysis," in *Proc. Design Automation and Test Conf. in Europe*, pp. 432–437, 2008.

[13] J. M. Wang and T. V. Nguyen, "Extended Krylov subspace method for reduced order analysis of linear circuit with multiple sources," in *ACM/IEEE DAC*, pp. 247–252, 2000.

[14] Y. Lee, Y. Cao, T. Chen, J. Wang, and C. Chen, "HiPRIME: Hierarchical and passivity preserved interconnect macromodeling engine for RLKC power delivery," *IEEE TCAD*, pp. 797–806, 2005.

[15] E.J.Grimme, *Krylov projection methods for model reduction (Ph. D Thesis)*. Univ. of Illinois at Urbana-Champaign, 1997.

[16] A. Odabasioglu, M. Celik, and L. Pileggi, "PRIMA: Passive reduced-order interconnect macro-modeling algorithm," *IEEE TCAD*, pp. 645–654, 1998.

[17] P. Feldmann and F. Liu, "Sparse and efficient reduced order modeling of linear sub-circuits with large number of terminals," in *IEEE/ACM ICCAD*, 2004.

[18] P. Liu, S. X.-D. Tan, J. Kong, B. McGaughy, and L. He, "Efficient method for terminal reduction of interconnect circuits considering delay variations," in *IEEE/ACM ICCAD*, 2005.

[19] K. J. Kerns and A. T. Yang, "Stable and efficient reduction of large, multiport RC network by pole analysis via congruence transformations," *IEEE TCAD*, pp. 734–744, 1998.

[20] X. Li, P. Li, and L. Pileggi, "Parameterized interconnect order reduction with explicit-and-implicit multi-parameter moment matching for inter/intra-die variations," in *IEEE/ACM ICCAD*, 2005.

[21] G. H. Golub and C. F. V. Loan, *Matrix Computations*. Baltimore, MD: The Johns Hopkins University Press, 3 ed., 1989.

[22] M. Berry, "Large scale singular value computations," *Int. J. of Supercomputer Appl.*, pp. 13–49, 1992.

[23] M. Band, "Incremental singular value decomposition of uncertain data with missing values," in *European Conf. on Computer Vision*, 2002.